chemosensors

MDPI

Supporting Information

Pyridinyl Conjugate of UiO-66-NH_2 as Chemosensor for the Sequential Detection of Iron and Pyrophosphate Ion in Aqueous Media

Aasif Helal [1,*], Md. Eyasin Arafat [1] and Mohammad Mizanur Rahman [2]

[1] Center of Research Excellence in Nanotechnology, King Fahd University of Petroleum and Minerals, Dhahran 31261, Saudi Arabia; g201707550@kfupm.edu.sa

[2] Center of Research Excellence in Corrosion, King Fahd University of Petroleum & Minerals, Dhahran 31261, Saudi Arabia; mrahman@kfupm.edu.sa

* Correspondence: aasifh@kfupm.edu.sa; Tel.: +966-013-860-7532

Received: 7 October 2020; Accepted: 23 November 2020; Published: date

1. Characterization of H_2L

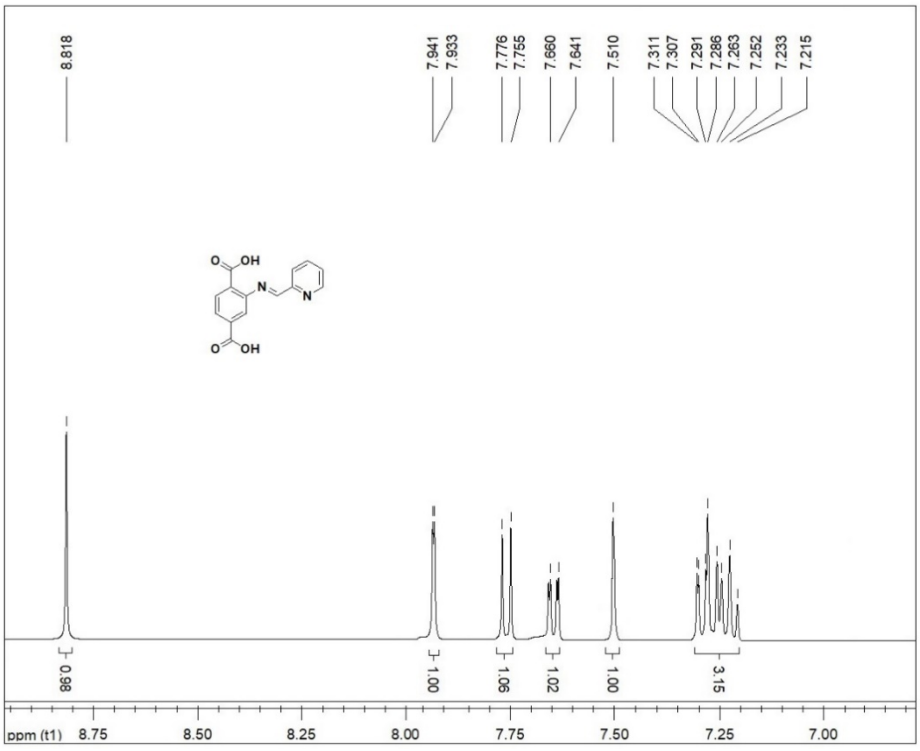

Figure S1. ^{1}H NMR spectrum of **H_2L** in DMSO-d_6 solution at 400 MHz.

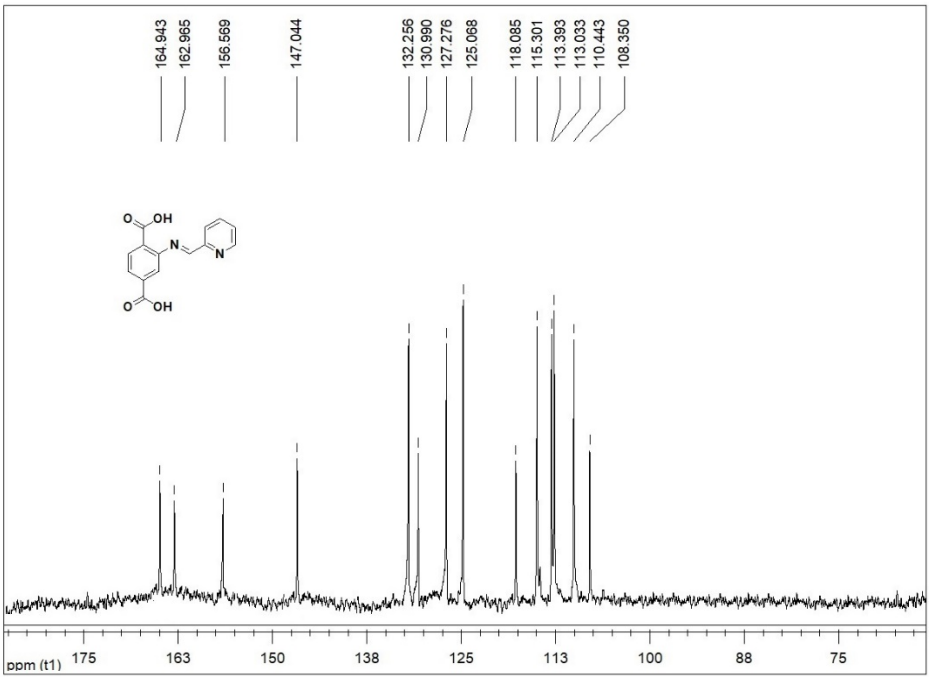

Figure S2. ^{13}C NMR spectrum of **H_2L** in DMSO-*d*$_6$ solution at 400 MHz.

2. Characterization of UiO-66-N-Py

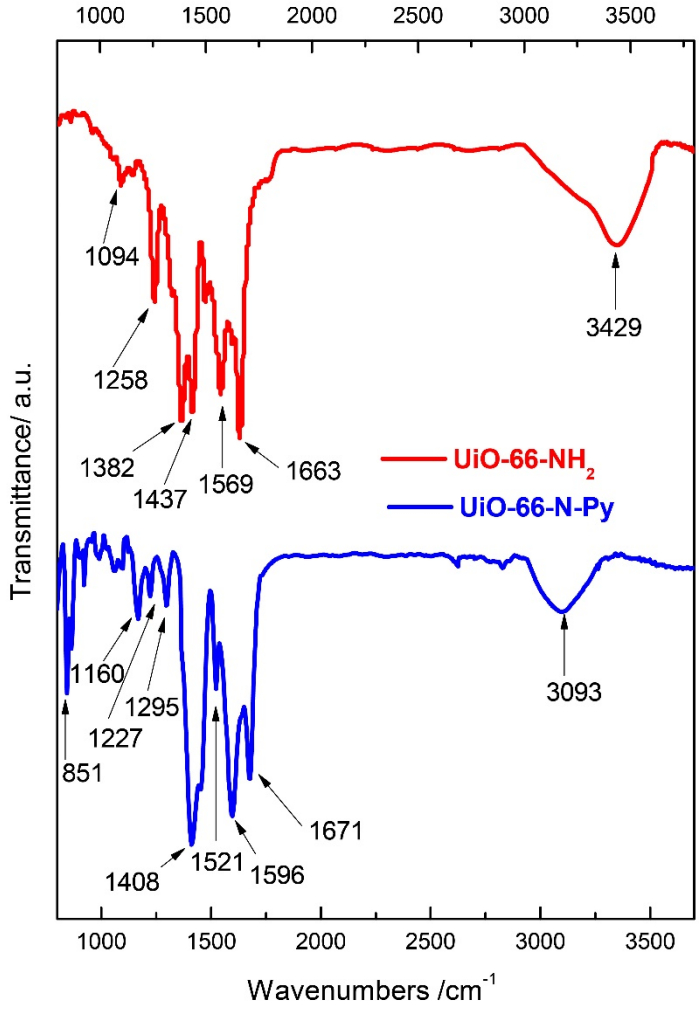

Figure S3. FTIR spectra of UiO-66-N-Py and UiO-66-NH_2.

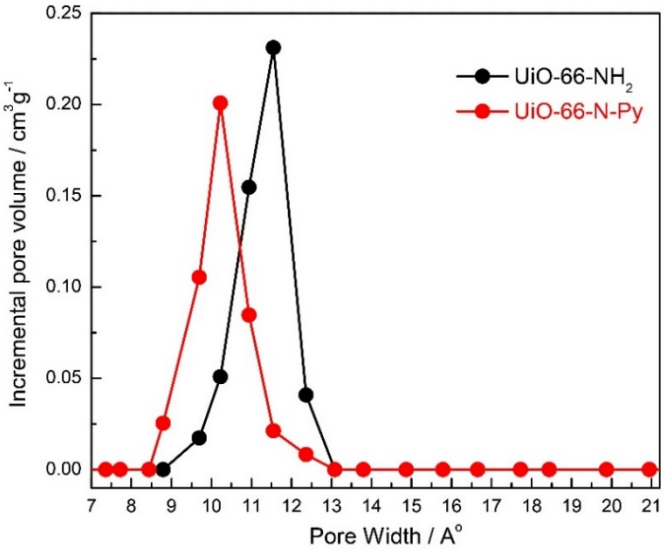

Figure S4. DFT adsorption pore-size distribution of UiO-66-N-Py and UiO-66-NH2.

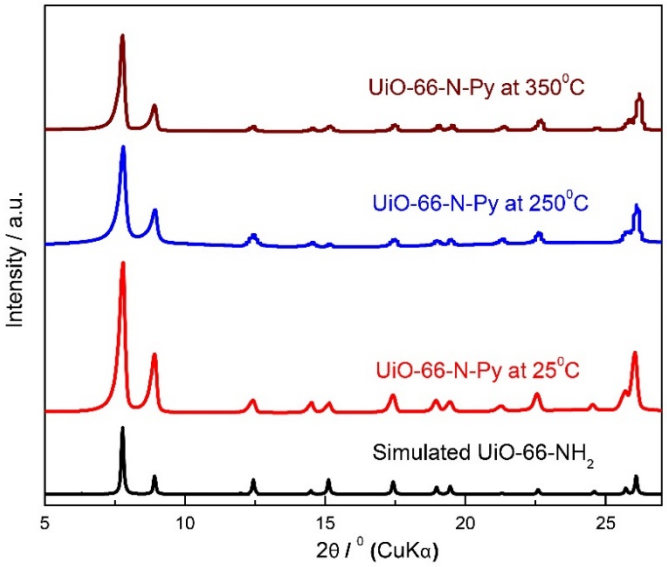

Figure S5. Thermal stability of UiO-66-N-Py at different temperatures.

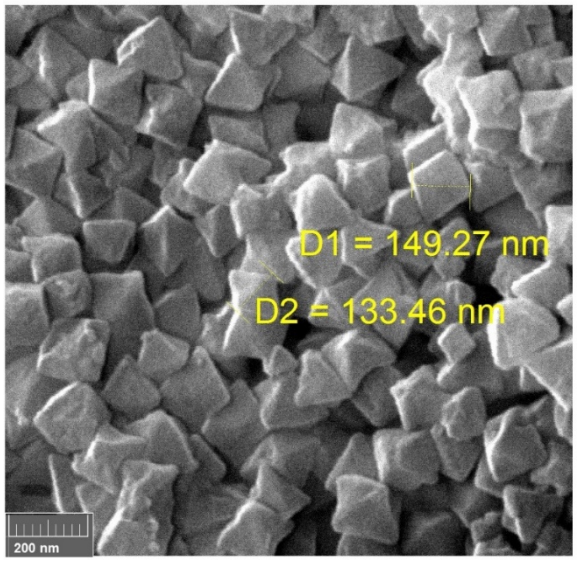

Figure S6. SEM image of UiO-66-N-Py.

3. Emission Properties of UiO-66-N-Py

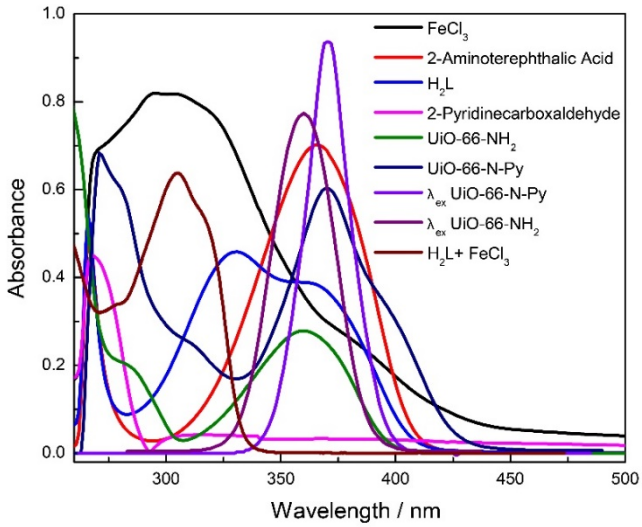

Figure S7. UV-vis spectra of UiO-66-N-Py, UiO-66-NH_2, linkers, and $FeCl_3$ in water.

The emission spectra were corrected for the inner filter effect by using the following correction factor:

$$F_{corr} = F_0 x 10^{(A_{ex} l_{ex} + A_{em} l_{em})} \quad (1)$$

where F_{corr} is the corrected fluorescence intensity, A_{ex} is the absorbance at the excitation wavelength, l_{ex} is the penetration depth of the light into the sample, A_{em} is the absorbance over the emission wavelength and l_{em} is the emission path length [1].

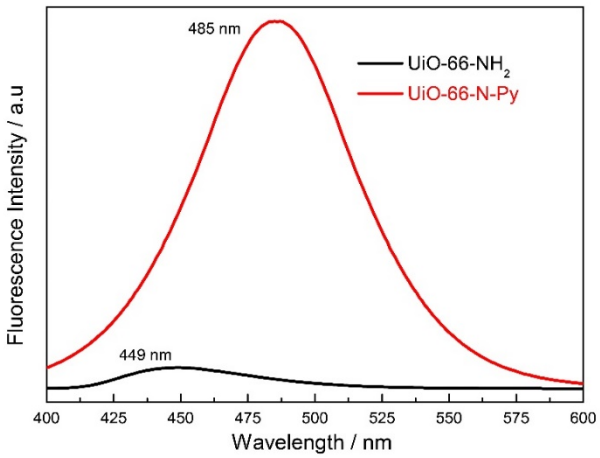

Figure S8. The fluorescence emission spectra of UiO-66-NH_2 and UiO-66-N-Py. (λ_{ex} = 341nm).

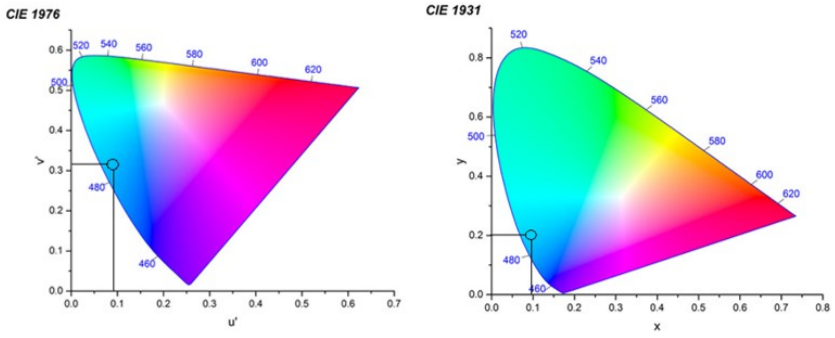

Figure S9. Chromaticity diagram of UiO-66-N-Py dispersion in water.

4. Cation Sensing Properties of UiO-66-N-Py

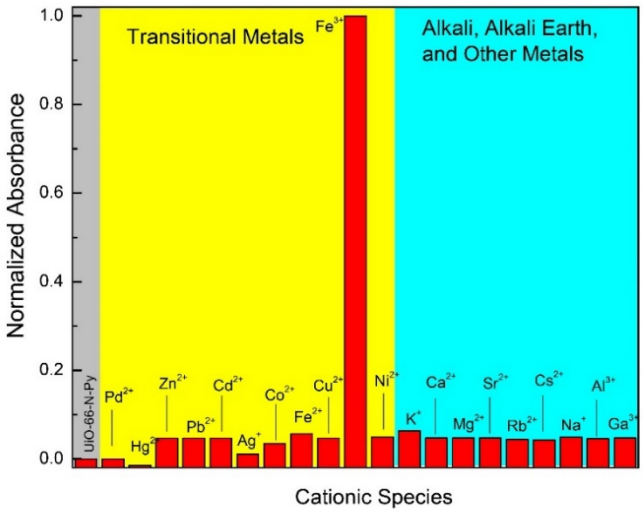

Figure S10. Change in the normalized absorbance of UiO-66-N-Py at 315 in water upon addition of 200 μL of different metal cations (10^{-2} M).

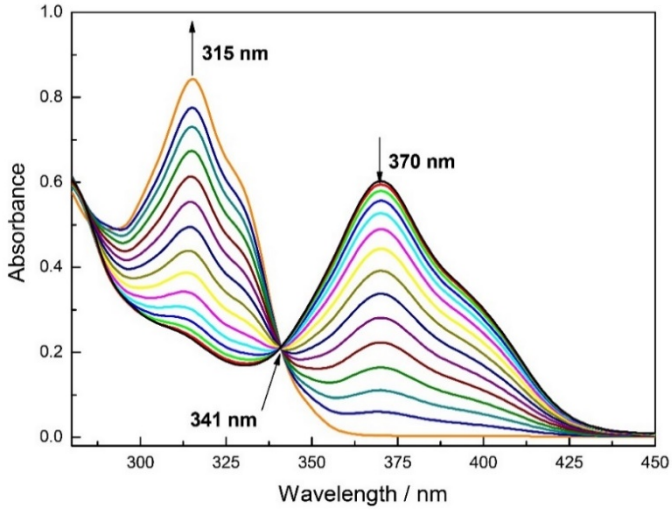

Figure S11. Changes in UV-vis spectra of UiO-66-N-Py with the incremental addition of $FeCl_3$ (10^{-2} M) in water.

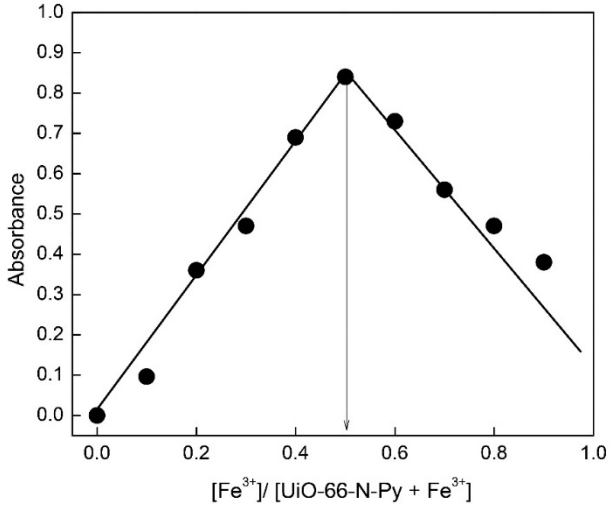

Figure S12. Job's plot for UiO-66-N-Py with $FeCl_3$ in water.

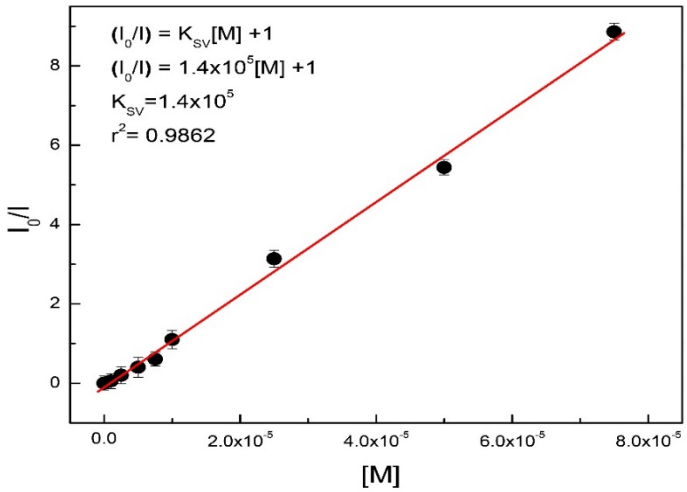

Figure S13. Stern-Volmer plot of UiO-66-N-Py quenched by $FeCl_3$ in water.

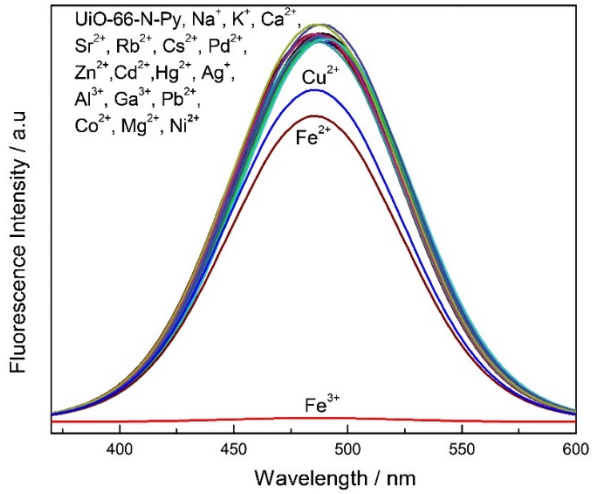

Figure S14. Changes in emission spectra of UiO-66-N-Py upon addition of 200 μL of different metal cations (10^{-2} M) in water. (λ_{ex} = 341 nm).

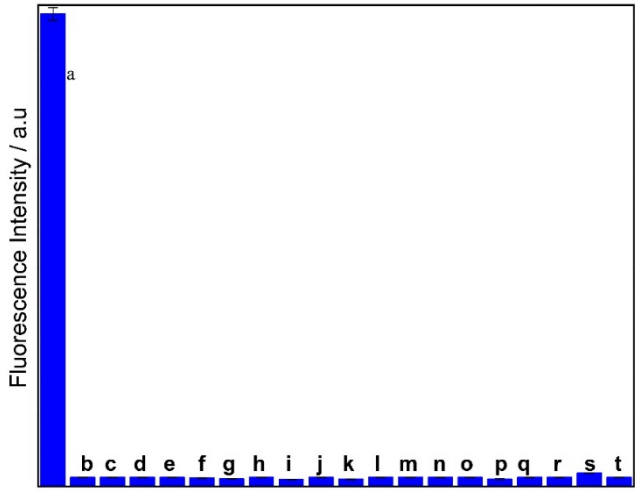

Figure S15. Competitive metal ion selectivity of UiO-66-N-Py: Bars indicate the fluorescence intensity (341 nm excitation, 485 nm emission). Salts of various metal ions (10^{-2} M) were added to UiO-66-N-Py and Fe^{3+} (10^{-2} M) (a) UiO-66-N-Py only, (b) $Ag^+ + Fe^{3+}$, (c) $Pb^{2+} + Fe^{3+}$, (d) $Zn^{2+} + Fe^{3+}$, (e) $Mg^{2+} + Fe^{3+}$, (f) $Fe^{3+} + Cu^{2+}$, (g) $K^+ + Fe^{3+}$, (h) $Co^{2+} + Fe^{3+}$, (i) $Al^{3+} + Fe^{3+}$, (j) $Fe^{2+} + Fe^{3+}$, (k) $Na^+ + Fe^{3+}$, (l) $Cd^{2+} + Fe^{3+}$, (m) $Sr^{2+} + Fe^{3+}$, (n) $Rb^+ + Fe^{3+}$, (o) $Pd^{2+}+ Fe^{3+}$ (p) $Ni^{2+} + Fe^{3+}$, (q) $Hg^{2+} + Fe^{3+}$, (r) $Ga^{3+} + Fe^{3+}$, (s) $Cs^+ + Fe^{3+}$, (t) $Ca^{2+} + Fe^{3+}$ in water.

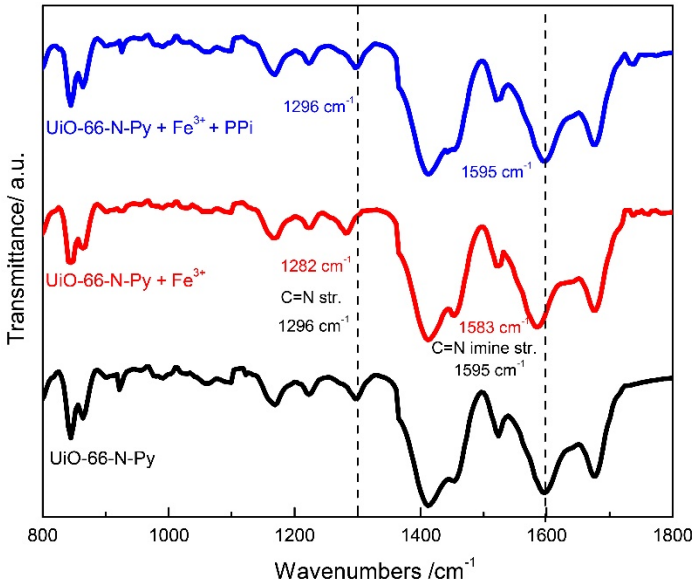

Figure S16. Part of FTIR spectra for UiO-66-N-Py before and after sensing experiments with Fe^{3+}.

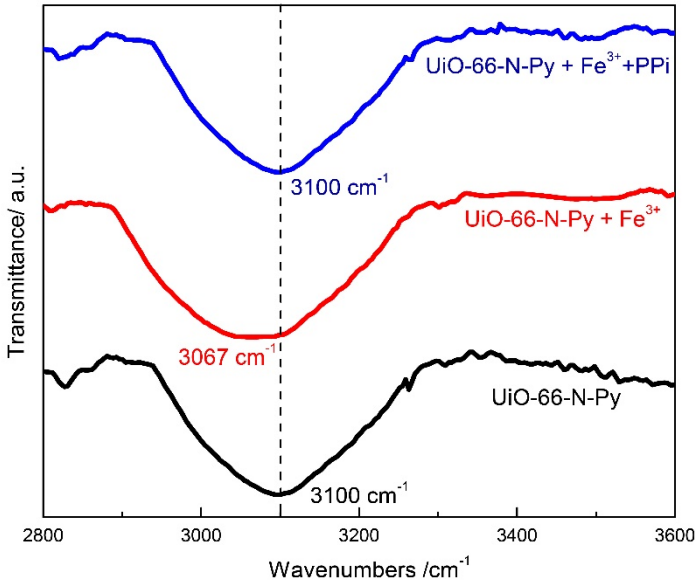

Figure S17. Part of FTIR spectra for UiO-66-N-Py before and after sensing experiments with $Fe^{3+}$and PPi.

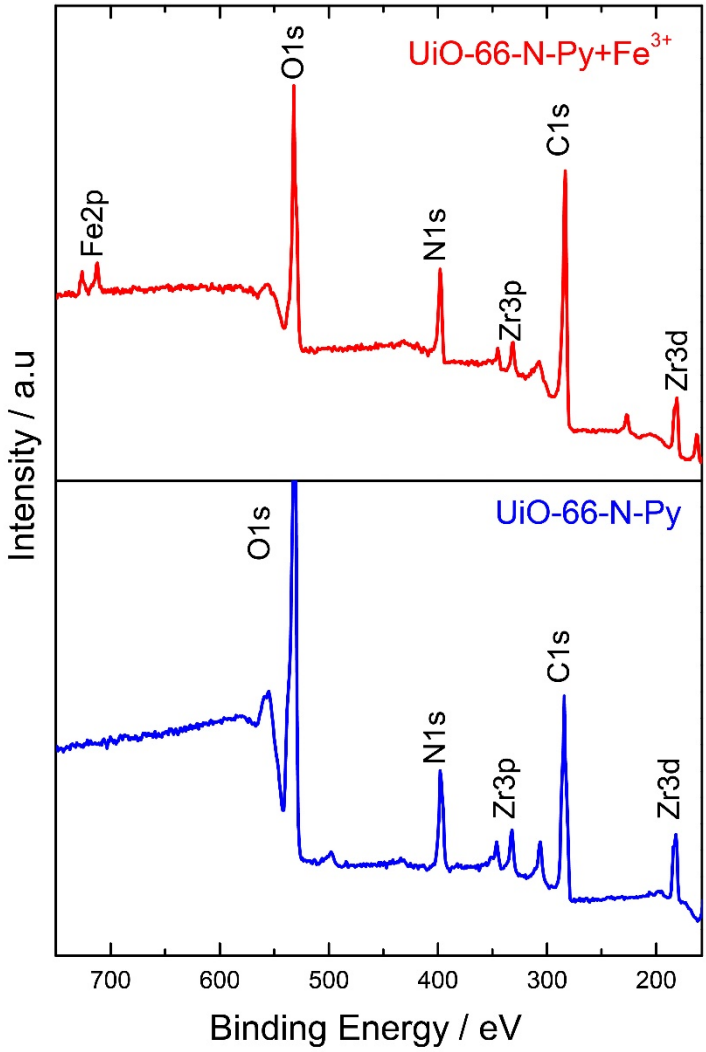

Figure S18. XPS of UiO-66-N-Py and UiO-66-N-Py+Fe^{3+}.

5. Anion Sensing Properties of UiO-66-N-Py+Fe^{3+}

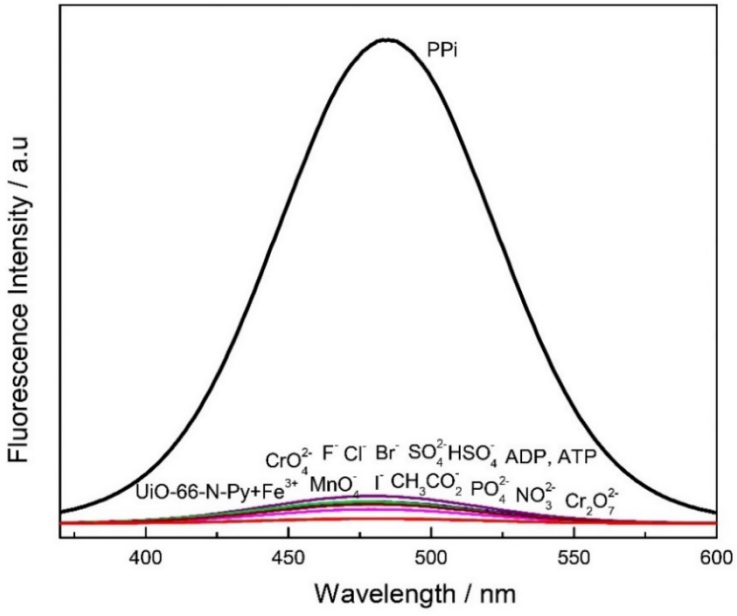

Figure S19. Changes in emission spectra of UiO-66-N-Py-Fe^{3+} upon addition of 200 μL of different anionic species (10^{-2} M) in water. (λ_{ex} = 341 nm).

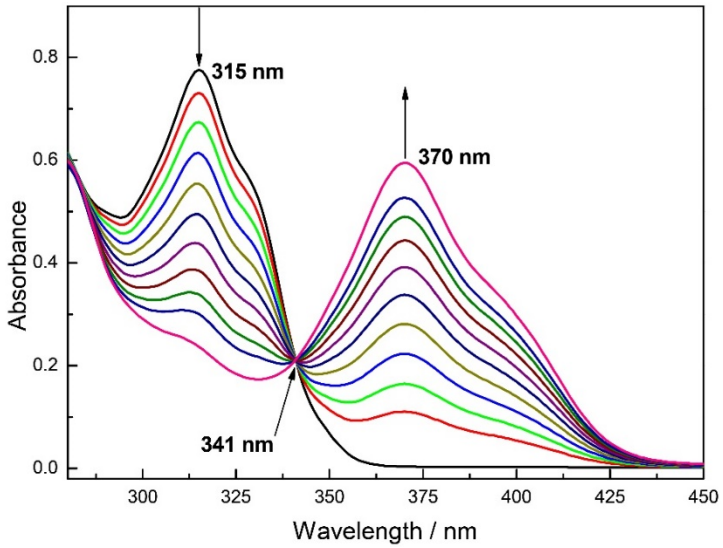

Figure S20. Changes in UV-vis spectra of UiO-66-N-Py+Fe^{3+} with the incremental addition of PPi (10^{-2} M) in water.

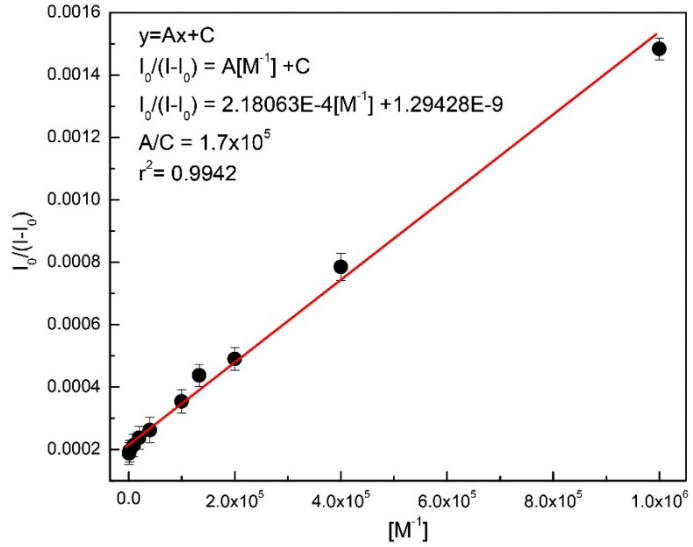

Figure S21. Binding constant calculation of UiO-66-N-Py+Fe^{3+} with PPi in water.

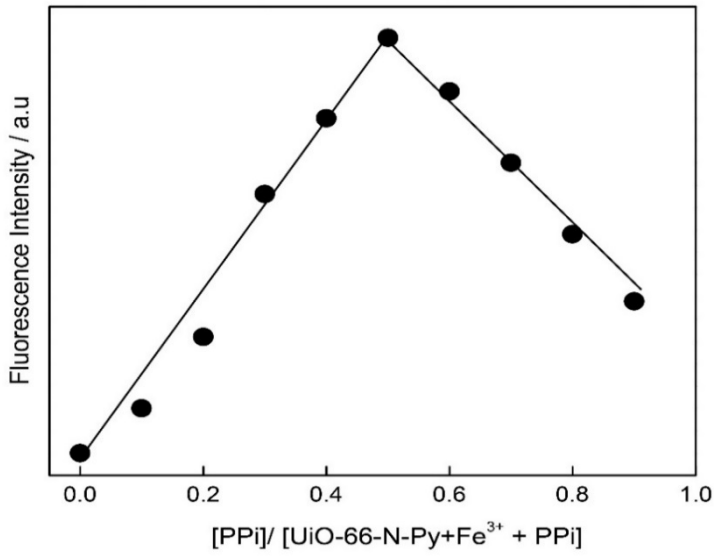

Figure S22. Job's plot for UiO-66-N-Py + Fe^{3+} with PPi in water.

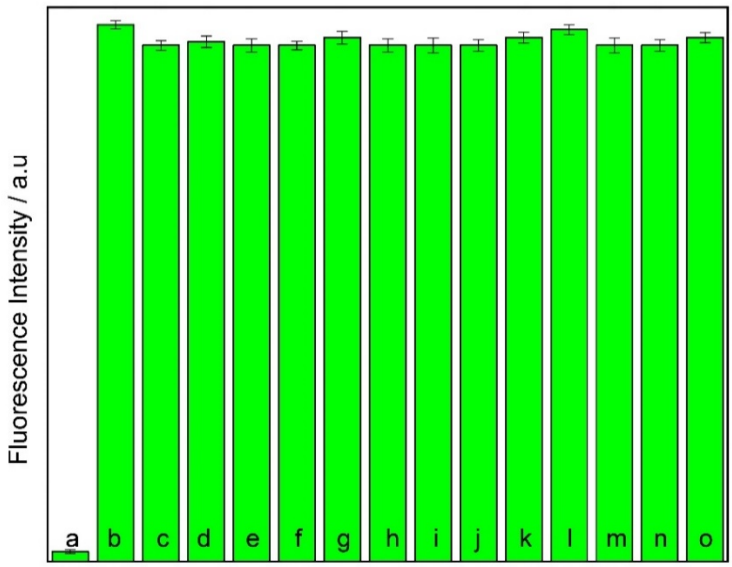

Figure S23. Competitive anion selectivity of UiO-66-N-Py+Fe^{3+}: Bars indicate the fluorescence intensity (341 nm excitation, 485 nm emission). Various anions (10^{-2} M) were added to UiO-66-N-Py+$Fe^{3+}$and PPi (10^{-2} M) (a) UiO-66-N-Py+Fe^{3+} only, (b) F^- + PPi, (c) Cl^- + PPi, (d) Br^- + PPi, (e) I^- + PPi, (f) $CH_3CO_2^-$ + PPi, (g) MnO_4^- + PPi, (h) NO_3^{2-} + PPi, (i) PO_4^{2-} + PPi, (j) SO_4^{2-} + PPi, (k) HSO_4^- + PPi, (l) $Cr_2O_7^{2-}$ + PPi, (m) CrO_4^{2-} + PPi, (n) ADP + PPi, (o) ATP + PPi in water.

6. Determination of the detection limit [2]

The detection limit was calculated based on the fluorescence quenching titration experiments. The fluorescence emission spectrum of UiO-66-N-Py and UiO-66-N-Py+Fe^{3+} was measured six times from which the standard deviation of the blank measurement was achieved. To gain the slope, the fluorescence intensity at 485 nm was plotted as a concentration of the analytes. So the detection limit was calculated with the following equation:

$$\text{Detection limit} = 3\sigma/k \quad (2)$$

where σ is the standard deviation of blank measurement, k is the slope between the normalized fluorescence intensity versus analytes concentrations.

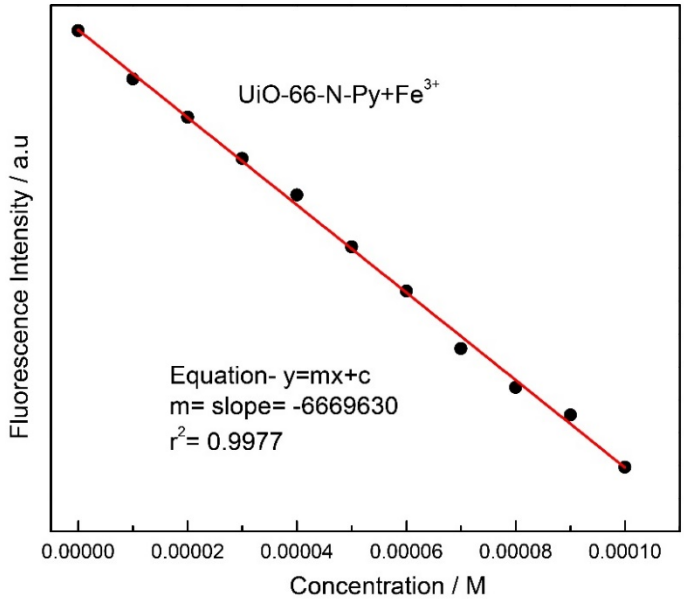

Figure S24. Linear region of fluorescence intensity (λ_{ex} = 341 nm and λ_{em} = 485 nm) for UiO-66-N-Py suspensions in water upon incremental addition of Fe^{3+} solutions.

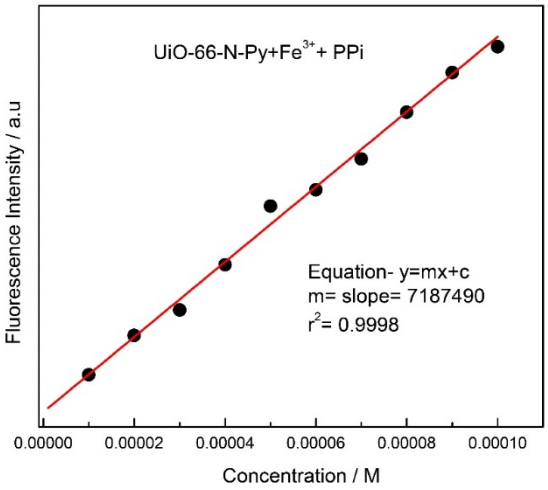

Figure 25. Linear region of fluorescence intensity (λ_{ex} = 341 nm and λ_{em} = 485 nm) for UiO-66-N-Py+Fe^{3+} suspensions in water upon incremental addition of PPi solutions.

Table 1. Calculation of the Limit of Detection (LOD).

	Blank Readings	Fe^{3+}	PPi
1	Fluorescence Intensity	1027.495	19.23888
2	Fluorescence Intensity	1027.305	19.74356
3	Fluorescence Intensity	1027.525	19.94235
4	Fluorescence Intensity	1028.195	20.3923
5	Fluorescence Intensity	1028.295	20.7681
6	Fluorescence Intensity	1028.095	20.9871
Standard Deviation (σ)		0.42415	0.72594
Slope (k)		6669630 ± 254861 μM	7187490 ± 364513 μM
Detection limit (3σ/k)		0.19 μM / 10 ppb	0.3 μM / 50 ppb

7. pH Properties of UiO-66-N-Py

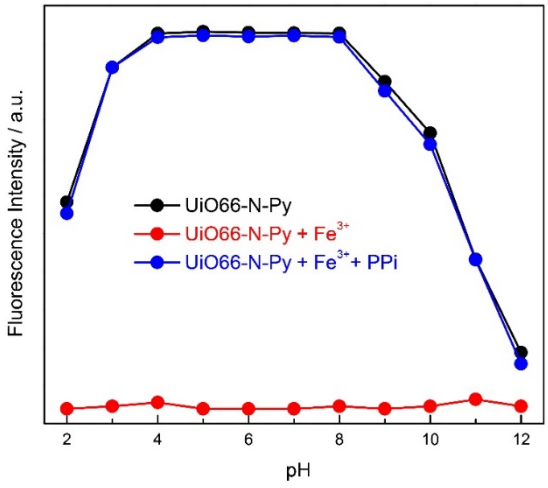

Figure S26. Effect of pH on the emission intensities at 485 nm of UiO-66-N-Py, in H_2O (λ_{ex} = 341 nm).

References:

1. Sunish, K.S.; Benjamin, R.; Ryan, P.S.; Jędrzej, S.; Kenneth, P.G.; Matthew F.P.; Ronald P.S. Photophysics of Untethered ZnTPP Fullerene Complexes in Solution. *J. Phys. Chem. A* **2011**, *115*, 12217–12227.
2. Lv, R.; Wang, J.; Zhang, Y.; Li, H.; Yang, L.; Liao, S.; Gu, W.; Liu, X. An amino-decorated dual-functional metal–organic framework for highly selective sensing of Cr(III) and Cr(VI) ions and detection of nitroaromatic explosives. *J. Mater. Chem. A* **2016**, *4*, 15494-15500.